Effects of intermetallic nanoparticles on the evolution of vacancy defects in electron-irradiated Fe–Ni–Al material

2006 J. Phys.: Condens. Matter 18 365

(http://iopscience.iop.org/0953-8984/18/2/002)

INSTITUTE OF PHYSICS PUBLISHING JOURNAL OF PHYSICS: CONDENSED MATTER

J. Phys.: Condens. Matter **18** (2006) 365–377 doi:10.1088/0953-8984/18/2/002

Effects of intermetallic nanoparticles on the evolution of vacancy defects in electron-irradiated Fe–Ni–Al material

A P Druzhkov[1], **D A Perminov and V L Arbuzov**

Institute of Metal Physics, Ural Branch RAS, 18 S Kovalevskaya Street, 620219 Ekaterinburg GSP-170, Russia

E-mail: druzhkov@imp.uran.ru

Received 5 May 2005, in final form 22 September 2005
Published 14 December 2005
Online at stacks.iop.org/JPhysCM/18/365

Abstract

In this paper we study the effects of intermetallic nanoparticles like Ni_3Al on the evolution of vacancy defects in the fcc Fe–Ni–Al alloy under electron irradiation using positron annihilation spectroscopy. It was shown that the nanosized (∼4.5 nm) intermetallic particles homogeneously distributed in the alloy matrix caused a several-fold decrease in the accumulation of vacancies as compared to their accumulation in the quenched alloy. This effect was enhanced with the irradiation temperature. The irradiation-induced growth of intermetallic nanoparticles was also observed in the pre-quenched Fe–Ni–Al alloy under irradiation at 573 K. Thus, a quantum-dot-like positron state in ultrafine intermetallic particles, which we revealed earlier, provided the control over the evolution of coherent precipitates, along with vacancy defects, during irradiation and annealing. Possible mechanisms of the absorption of point defects by coherent nanoparticles have been discussed too.

1. Introduction

Austenitic stainless steels have been adopted as candidate materials for fast breeder reactor core applications. Many efforts have been made to prolong their life by improving their strength at elevated temperatures and swelling resistance. For example, it is known that the duration of the incubation period of void swelling in those steels correlates with the time required for the redistribution of the alloying elements and the formation of the precipitate distribution. Moreover, it is frequently found that the material exhibits enhanced radiation resistance when precipitates are coherent with the matrix. The swelling resistance of PE 16 Nimonic [1] and other nickel-based alloys [2, 3] is attributed usually to the population of ultrafine precipitates like $Ni_3Al(Ti)$ (γ'-phase) homogeneously distributed in the matrix.

[1] Author to whom any correspondence should be addressed.

0953-8984/06/020365+13$30.00

The experimental papers cited here demonstrated that coherent precipitates reduce average concentrations of point defects, thereby suppressing the swelling process. However, the mechanism of point defect absorption by coherent particles is poorly understood in detail [4, 5]. Positron annihilation spectroscopy (PAS) can provide new information about the interaction between point defects and intermetallic particles.

Positrons have been well known as a sensitive probe for vacancy-type defects [6]. Furthermore, we have found recently that a positron can be 'trapped' by embedded ultrafine particles in materials, namely there is quantum-dot-like positron state in thermally aged fcc Fe–Ni–Al alloy [7]. A positron in this state annihilates only with an electron from intermetallic particles and provides site-selective information about their electronic and atomic structures in the form of two emitted γ-quanta. For example, intermetallic precipitates $\sim$2 nm in size, formed in Fe–34.2 wt% Ni–5.4 wt% Al by thermal ageing at 823 K for 22 h, have a structure of the Ni_3Al type with the addition of Fe atoms, are free from defects, three dimensional and have no open-volume defects at the interfaces which can trap the positron.

This study demonstrated that nanocrystalline particles like Ni_3Al reduce the accumulation of vacancy-type defects under irradiation. Nanosized intermetallic particles were formed during thermal ageing of an fcc Fe–Ni–Al alloy. The fcc Fe–Ni–Al (γ-phase) served as a model alloy of fast breeder reactor stainless steels. At early stages of ageing ultrafine precipitates of the γ'-phase were homogeneously distributed in the matrix and were fully coherent with it [7, 8]. Point defects were induced by electron irradiation, which generated homogeneously distributed Frenkel pairs.

Positron states in vacancy-type defects and intermetallic nanoparticles were diagnosed by angular correlation of annihilation radiation (ACAR), which is one of the positron annihilation techniques [9]. ACAR gives information on electronic properties of analysed materials, specifically the momentum distribution of valence and core electrons [10]. Core electrons are tightly bound to nuclei and, therefore, high-momentum parts of the ACAR spectrum carry information on the type of atoms in the region scanned by the positron [11–14]. Therefore the annihilation of trapped positrons with surrounding core electrons reveals chemical information. The present study also employs this approach for identifying the local chemical environment of positron annihilation sites.

2. Materials and methods

The Fe–Ni–Al (34.2 wt% Ni, 5.4 wt% Al, C $\leqslant$ 0.01 wt%, the balance Fe) fcc alloy was used. After rolling, cutting and electrical polishing, samples about 10×10 mm^2 in size (0.2–0.3 mm thick) were annealed under a 10^{-6} Pa vacuum at 1373 K for 1 h and quenched in water at room temperature (Q-state). The presence of one austenitic phase in the samples was checked by x-ray analysis. Some of the samples were thermally aged at 923 K for 3 h (A-state). The samples were also quenched in water after each thermal treatment. It is known [8] that low-temperature (823–923 K) ageing of Ni-based alloys leads to the nucleation and the growth of nanosized spherical particles of an ordered ($L1_2$)γ'-phase, which is coherent with the matrix.

The microstructure of the quenched and aged samples was certified using a JEM-200 CX transmission electron microscope at an accelerating voltage of 160 kV (TEM). Samples of the quenched alloys had grains $\sim$50 μm in size and a dislocation density of about 10^7 cm^{-2}. The TEM examination of the alloy which was aged at 923 K for 3 h revealed the presence of an ordered γ'-phase whose lattice was isomorphous to the lattice of the solid solution. The dimensions and the density of the spherical precipitates were determined from dark-field images recorded in superstructure reflections. The particles were $\sim$4.5 nm in size, their density was 1×10^{17} cm^{-3} and the volume fraction was $\sim$0.5%. The magnitude and the sign of the γ/γ'

lattice mismatch δ was defined as the relative difference of the two lattice parameters a_p and a_m of γ' precipitates and the γ matrix respectively, $\delta = (a_p - a_m)/a_m$. The lattice mismatch δ at room temperature was about +0.7% for the Fe–Ni–Al alloy [15]. The mismatch δ is responsible for the stress field in both the precipitates and the matrix through the coherent interface [16].

Samples of the Fe–Ni–Al alloy (in the Q-state and A-state) were irradiated at 300 to 573 K with 5 MeV electrons in a linear accelerator. The samples were positioned as tightly as possible in the centre of the irradiation zone (10×10 mm^2) of the sample holder and electron beam sweeping was applied to provide homogeneous irradiation. The irradiation temperature was controlled to within ± 5 K. The maximum electron fluence was 5×10^{18} cm^{-2}, which corresponded to the damaging dose of $(1–2) \times 10^{-4}$ dpa as calculated by the modified Kinchin–Pease model [17].

The irradiated samples were annealed stepwise (25–50 K per step) in a vacuum over the temperature interval from 300 to 900 K at an average heating rate of 1 K min^{-1}.

Samples of a well-annealed fcc Fe–36 wt% Ni (Fe–Ni) alloy and monocrystalline Ni_3Al–Fe compound were also used in the ACAR measurements as references. A monocrystalline compound with chemical composition $Ni_{71}Al_{21}Fe_8$ (in at.%) was grown by the Bridgman method (see [18] and references therein).

The ACAR method was realized in a one-dimensional ACAR spectrometer providing a resolution of 1 mrad $\times$ 160 mrad [19]. A ^{68}Ge positron source of activity of 350 MBq was used. At least 8×10^5 coincidence counts were collected in each ACAR spectrum; the peak-to-background ratio was $\sim 10^3$. The ACAR spectra represented the dependence of the coincidence count rate on the angle θ (θ being the deviation of annihilation γ-quanta from anticollinearity). The angle $\theta = p_z/m_0c$, where p_z is the transverse component of the momentum of an electron–positron pair, m_0 is the rest mass of an electron, and c is the velocity of light. The ACAR data contain information about the momentum distribution of annihilating electrons [10] and it is possible to separate contributions from annihilation of positrons with nearly free electrons (the low-momentum part of the spectrum) and core electrons (the high-momentum part of the spectrum). The lattice crystal field has little effect on strongly bound (core) electrons and, therefore, the high-momentum part of the ACAR spectrum bears information about the type of atoms at a positron annihilation site.

The ACAR spectra of the compound and the alloys were approximated by an inverted parabola and a Gaussian. The approximation of the experimental spectra considering the spectrometer resolution function has been described in detail elsewhere [20]. The approximation quality criterion approached unity.

The contribution of core electrons to the ACAR spectra was determined from ratio curves [12]. The latter were obtained in the following way: approximated ACAR spectra were normalized to a unit area and then Fe–Ni–Al and Ni_3Al–Fe spectra were divided by the spectrum of the reference alloy.

Changes in the shape of the ACAR spectra were also characterized by a standard S-parameter [19]. The S-parameter was defined as the ratio of the sum of the coincidence count rate at θ from 0 to 3.5 mrad to the full coincidence count rate. The S-parameter characterized the probability of annihilation of positrons with nearly free electrons. When positrons were trapped in open volume defects, the S-parameter increased [19]. According to the simple trapping model (STM) [21], the S-parameter is related to the concentration of defects (e.g., small vacancy clusters) C_{cl} as

$$C_{\mathrm{cl}} = \frac{\lambda_{\mathrm{f}}(S - S_{\mathrm{f}})}{\mu_{\mathrm{cl}}(S_{\mathrm{cl}} - S)}, \tag{1}$$

where λ_{f} is the positron annihilation rate in the bulk (free) state; μ_{cl} is the specific positron trapping rate; S_{f} and S_{cl} are S-parameters characteristic of the positron annihilation from

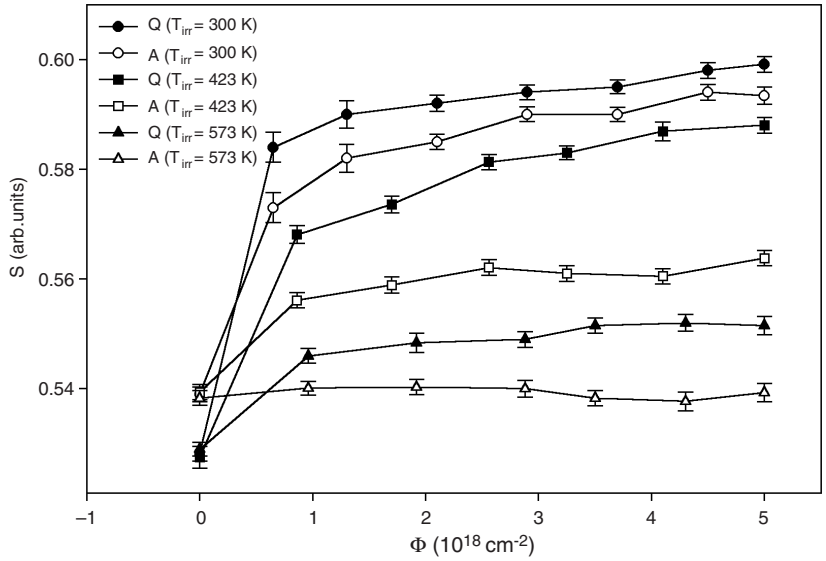

Figure 1. Variation of the *S*-parameter as a function of the electron fluence for the Fe–Ni–Al alloy in the quenched (Q) and aged (A) initial states. Irradiation temperatures are 300, 423 and 573 K, respectively.

the bulk (free) and defect-trapped states respectively. In the case of small three-dimensional vacancy clusters (VCs), $\mu_{cl} \approx n\mu_v$ [22] (n being the cluster multiplicity and μ_v the specific trapping rate for monovacancy). STM is correctly applicable to homogeneously distributed defects in materials (e.g., in the case of electron irradiation).

3. Results

3.1. Accumulation of vacancy defects

Figure 1 presents the dependence of the *S*-parameter on the electron fluence for Fe–Ni–Al alloys in initial quenched (Q) and aged (A) states exposed to irradiation at 300, 423 and 573 K respectively. In the initial state (before irradiation) values of the *S*-parameter are larger in aged samples of the alloy. This is due to the quantum-dot confinement of positrons in intermetallic nanoparticles. About 98% positrons annihilate in nanoparticles as estimated in terms of the diffusion-limited trapping model [7]. As the fluence increases, the *S*-parameter grows whatever the initial state.

Let us consider first the behaviour of the *S*-parameter in the Q-series samples. Whatever the irradiation temperature, the dependence $S(\Phi)$ exhibits the following trend: (a) the *S*-parameter increases considerably as the fluence rises to 1.5×10^{18} cm^{-2}; (b) the *S*-parameter increases insignificantly at higher fluence values. Thus, a quasi-steady state [23] is established at a fluence larger than 1.5×10^{18} cm^{-2}. It was demonstrated earlier [24] that vacancies are mobile at room temperature in fcc Fe–Ni alloys of the invar composition. The increment of the *S*-parameter at the irradiation temperature of 300 K is due to trapping of positrons in small three-dimensional VCs. The concentration and the structure of VCs change little in the quasi-steady state.

As the temperature is elevated, interstitial atoms and vacancies become more mobile and, correspondingly, the probability of both the mutual recombination of point defects and

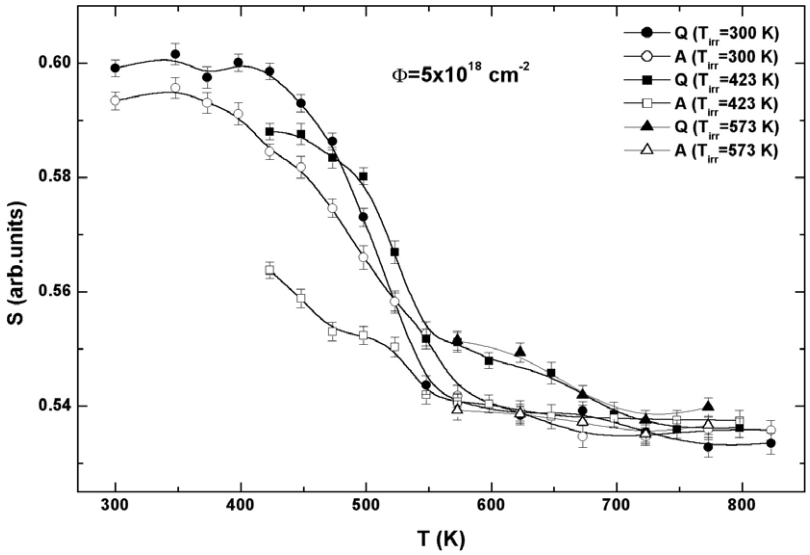

Figure 2. Evolution of the *S*-parameter as a function of the isochronal annealing temperature in 5×10^{18} cm^{-2} electron-irradiated Fe–Ni–Al (Q) and Fe–Ni–Al (A) at 300, 423, 573 K, respectively.

their absorption on sinks increases [23]. As a result, the concentration of accumulated VCs drops and the *S*-parameter acquires smaller values with growing irradiation temperature (see figure 1). It should be noted also that the configuration of VCs changes too as the irradiation temperature rises. For example, if the irradiation temperature is 573 K, prevailing clusters are two-dimensional VCs [24], for which the *S*-parameter is smaller than its counterpart for three-dimensional VCs.

The behaviour of the dependence $S(\Phi)$ in the aged alloys (series A) is similar to the behaviour of the *S*-parameter in the quenched alloys. However, the plateaus which are reached by the *S*-parameter are much lower, and this effect is enhanced as the irradiation temperature rises. If the irradiation temperature is 573 K, the value of the *S*-parameter changes little with the fluence. Thus, the presence of homogeneously distributed nanoparticles in the alloy matrix limits the increments of the *S*-parameter under irradiation.

3.2. Annealing of vacancy defects

Figure 2 presents the *S*-parameter versus the isochronal annealing temperature of the Q- and A-series alloys exposed to a fluence of up to 5×10^{18} cm^{-2}.

Let us analyse the behaviour of the *S*-parameter during annealing of the Q-series alloys. The *S*-parameter begins decreasing quickly at annealing temperatures above 420 K and the decrease nearly stops by 600 K in the alloy which was irradiated at room temperature. The quick drop of the *S*-parameter is due to the dissociation of VCs. The *S*-parameter of the alloy irradiated at 423 K begins decreasing nearly at the same annealing temperatures, but the drop of the *S*-parameter decelerates at temperatures above 550 K. The slow drop of the *S*-parameter at temperatures from 550 to 750 K is connected with annealing of thermally more stable two-dimensional configurations of vacancy clusters, which appeared either during irradiation at 423 K or during annealing as a result of the conversion of three-dimensional configurations of VCs to their two-dimensional configurations. Indeed, the *S*-parameter of the alloy irradiated

at 573 K behaves analogously to the S-parameter at the high-temperature stage of recovery in the alloy irradiated at 423 K. Notice also the growth of the S-parameter in the quenched alloy which was irradiated at 573 K and annealed at 773 K (see figure 2). The S-parameter increases due to 'trapping' of positrons by intermetallic particles, which are formed owing to radiation-induced ageing. This situation will be discussed in more detail below.

The S-parameter of the A-series alloys decreases at lower annealing temperatures. For example, the decrease of the S-parameter of the sample irradiated at 300 K begins at 360 K and ends by 600 K. The S-parameter of the aged alloy which was exposed to irradiation at 423 K decreases continuously and this decrease stops by 550 K. The stage above 550 K, which is connected with annealing of two-dimensional VCs, is absent here, in contrast to the Q-series sample. The S-parameter of the sample irradiated at 573 K does not change with the annealing temperature (see figure 2).

Thus, nanoparticles also influence the recovery of the S-parameter values during isochronal annealing of the irradiated samples. However, the S-parameter recovery also depends on the initial concentration of vacancy defects, which is much smaller than in the Q-series alloys.

4. Discussion

4.1. Dominating trapping centres of positrons in the irradiated alloys

Before we discuss the effect of nanoparticles on the evolution of vacancy defects, it is necessary to analyse which positron trapping centres dominate in irradiated Fe–Ni–Al alloys having initial Q- and A-states. Obviously, small VCs will be the only trapping centres in pre-quenched alloys (at least at irradiation temperatures of 300 and 473 K). In pre-aged alloys positrons are 'trapped' by nanoparticles in addition to vacancy clusters [7]. The physical mechanism responsible for positron confinement in nanoparticles is different than in the case of vacancy defects. Positron localization in nanoparticles results from the strong positron affinity of nanoparticle relative to host [25], while vacancy trapping is due to missing ionic core (cores) and a decreased electron density associated with an open volume defect. It is known that vacancy clusters represent deep traps (for example, the binding energy of a positron in small three-dimensional VCs in Ni equals 6–7 eV [26]), whereas a deep potential well for quantum-dot type structures is not more than 1–3 eV [27, 28]. One may expect therefore that trapping of positrons at vacancy clusters will dominate if the concentrations of the nanoparticles and VCs are comparable. Ratio curves [29] are most informative if types of trapping centres are analysed. The low-momentum part ($<5 \times 10^{-3}\ m_0c$) suggests trapping of positrons at vacancy defects, while the high-momentum part ($p_z \geqslant 10 \times 10^{-3}\ m_0c$) points to the local chemical environment of the annihilation site. The ratio curves of ACAR spectra for Fe–Ni–Al alloys were obtained with respect to the ACAR spectrum of well-annealed Fe–Ni alloy.

Irradiation at 300 K. Figure 3(a) presents ratio curves for Fe–Ni–Al in the initial state and after exposure to low and high fluences. The same figure contains a curve for a Ni_3Al–Fe (bulk) single crystal. The curve for the initial Q-state coincides with the curve obtained for Fe–Ni. Aluminium atoms in the solid solution have little effect on the annihilation parameters. The shape of the ratio curve for the A-state approaches the shape of the curve obtained for the Fe-containing bulk intermetallic. It was noted in section 3.1 and [7] that this effect is due to positron confinement in the nanoparticles. The enhancement in the high-momentum part (larger than $15 \times 10^{-3}\ m_0c$) is explained by the fact that positrons annihilate predominantly with core electrons of Ni atoms in Ni_3Al [7].

The ratio curves which were obtained for alloys exposed to small and large fluences are similar irrespective of the initial state of the alloys. Indeed, irradiation of the Fe–Ni–

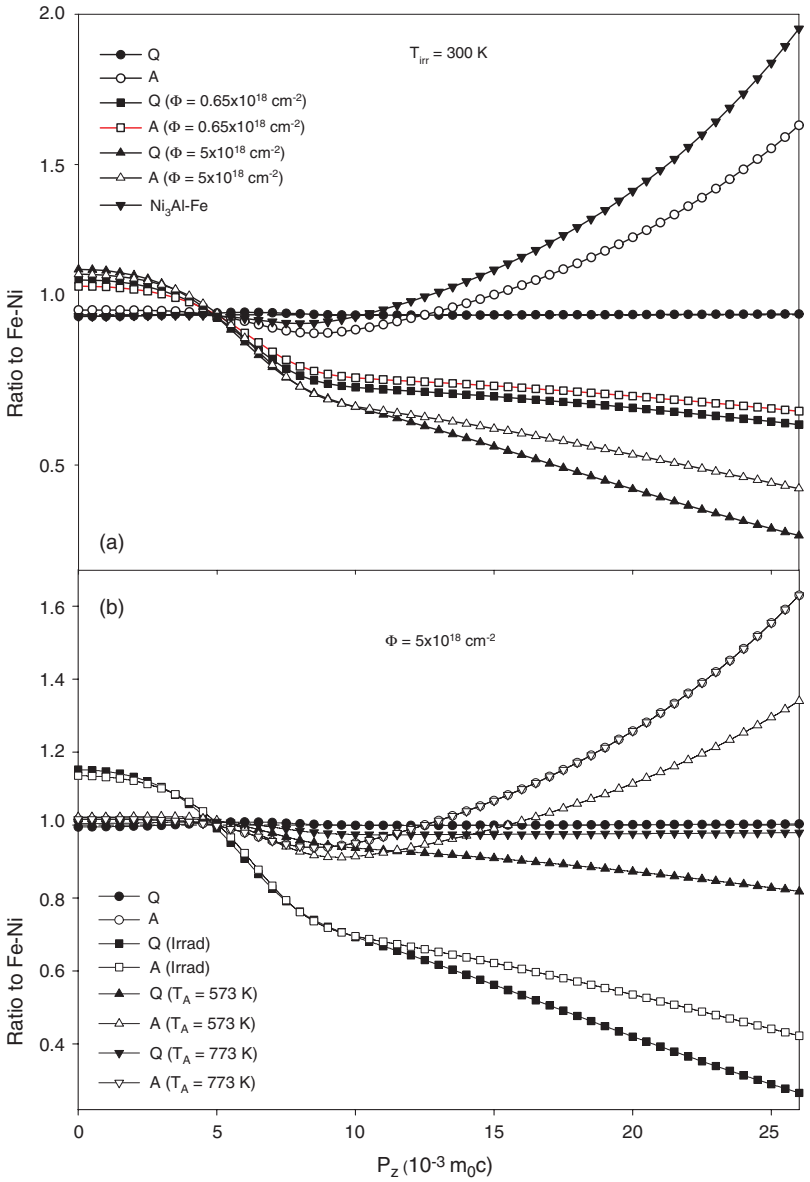

Figure 3. (a) Ratio curves of the ACAR spectra of the Fe–Ni–Al alloys as quenched (Q), after ageing (A), and as irradiated with different electron fluences at 300 K with respect to that of Fe–Ni. The ratio curve for the Ni_3Al–Fe compound is also presented. (b) Ratio curve variations versus annealing temperature in irradiated Fe–Ni–Al alloys (initial Q- and A-states) at 300 K. For details see the text.

(This figure is in colour only in the electronic version)

Al alloys sharply increases the probability of annihilation with nearly free electrons and, correspondingly, decreases the probability of annihilation with core electrons (see figure 3(a)). Such a situation is typical for positrons being trapped at open volume defects [7, 30]. One may think that dominant trapping centres in the Q- and A-alloys, which were irradiated at room

temperature, are sub-nanosized VCs homogeneously distributed in the matrix. Insignificant differences of the ratio curves are explained by the effect of the VCs concentration.

According to STM estimates (equation (1)), the concentration of vacancies in VCs in the A-alloy is half that in the Q-alloy (at the fluence of 5×10^{18} cm^{-2}). The annihilation rate in the Q-alloy was determined according to a linear interpolation of the τ_f^{-1} values of the constituent pure metals Fe, Ni and Al [31]. It was equal to 9.6×10^9 s^{-1}. The μ_v value was taken equal to 2.4×10^{-8} cm^3 s^{-1} (2.2×10^{15} s^{-1} at.) for pure Ni [32] as a typical value for fcc materials [33, 34]. The S_{cl} value was 0.605 [35].

If the average multiplicity of the clusters is assumed to be $n = 5$, $C_{cl} \sim 4 \times 10^{17}$ cm^{-3} in the A-alloy, i.e. the concentration of VCs is four times larger than the density of the nanoparticles. Obviously, being deeper traps, VCs will dominate.

The recovery of the ratio curves during annealing is shown in figure 3(b). The ratio curves for the irradiated alloys which were annealed at 773 K coincide with those for the Q- and A-states respectively. It may be inferred therefore that the atomic structure of the nanoparticles did not change in the aged alloy during irradiation and subsequent annealing. Ageing of the quenched alloy, which would be accompanied by the formation of nanoparticles under irradiation and subsequent annealing up to 773 K, was not detected (within the sensitivity limit of the method).

Irradiation at 423 K. Figure 4 shows the evolution of the ratio curves during irradiation and subsequent annealing of the alloys similarly to figure 3. In contrast to the results for irradiation at 300 K, the ratio curves for the alloys in Q- and A-states differ in their shape at small fluences (see figure 4(a)). The curve for the alloy A is similar to the initial curve, i.e. 'trapping' of positrons in nanoparticles dominates at small fluences. If the fluence is 5×10^{18} cm^{-2}, the curve for the alloy in the A-state corresponds more to trapping of positrons at VCs (its shape is similar to the shape of the curves obtained at a small fluence and $T_{irr} = 300$ K; see figure 3(a)). It may be assumed therefore that trapping of positrons at VCs dominates in the alloy in the A-state exposed to a high fluence. In this case, the STM estimates show that the concentration of accumulated vacancies in the alloy A is four times smaller than in the alloy Q (given the same fluence of 5×10^{18} cm^{-2}). If it is assumed that three-dimensional VCs are formed predominantly at $T_{irr} = 423$ K, then $C_{cl} \sim 6 \times 10^{16}$ cm^{-3} in the alloy A at the multiplicity $n = 5$. Although the VC concentration is smaller than the density of nanoparticles, the sensitivity of positrons to vacancy clusters as deeper traps is higher.

The ratio curves regain their initial shapes during annealing (see figure 4(b)). No changes are observed in the structure of the nanoparticles similarly to the case of irradiation at lower temperature. Ageing of the quenched alloy is not detected during irradiation and subsequent annealing either.

Irradiation at 573 K. At this temperature the values of the S-parameter of the alloy in the A-state depend little on the fluence, while the S-parameter of the alloy in the Q-state increases insignificantly with the fluence (see figure 1). Let us refer to the ratio curves in order to understand what processes take place in these alloys. Figure 5(a) presents the ratio curves for alloys Q and A exposed to different fluences. In the initial Q-state the curve exhibits a small increase in the intensity relative to 1 in the high-momentum part. This feature points to the initial stage of the alloy decomposition. It is known [36, 37] that nuclei of a high-density ($\sim 10^{20}$ cm^{-3}) ordered Ni_3Al phase may be formed owing to a low thermal conductivity and a finite thickness of samples during quenching from the homogenization temperature. Indeed, thicker ($\sim$0.25 mm) samples were used in this treatment series. Considering that the effect of the nuclei is small compared to the effect of nanoparticles, the radius of the nuclei may be assumed to be smaller than the critical radius (see [7] and references therein), i.e. the nuclei do not ensure a complete confinement of positrons.

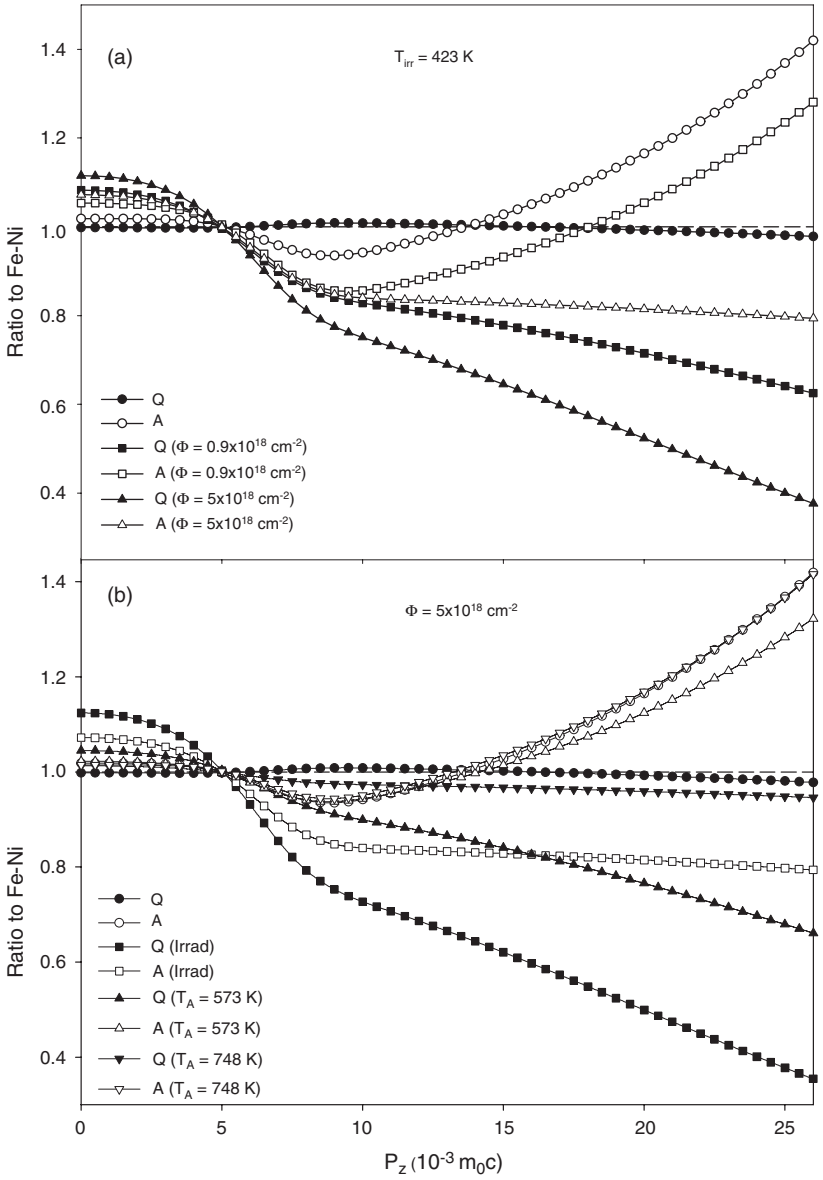

Figure 4. (a) Ratio curves of the ACAR spectra of the Fe–Ni–Al alloys as quenched (Q), after ageing (A), and as irradiated with different electron fluences at 423 K with respect to that of Fe–Ni. (b) Ratio curve variations versus annealing temperature in irradiated Fe–Ni–Al alloys (initial Q- and A-states) at 423 K. For details see the text.

The curves for the irradiated alloys in the Q-state characterize trapping of positrons at vacancy-type defects, i.e. thermally stable vacancy agglomerates are formed under irradiation. At the same time, trapping of positrons in nanoparticles dominates in alloy A. An interesting feature should be noted. The intensity of the curve at $p_z \geqslant 15 \times 10^{-3}\ m_0c$ considerably diminishes after exposure to a small fluence (0.9×10^{18} cm^{-2}) as compared to its intensity in the initial A-state. The curves returned to the initial A-state when the fluence increased

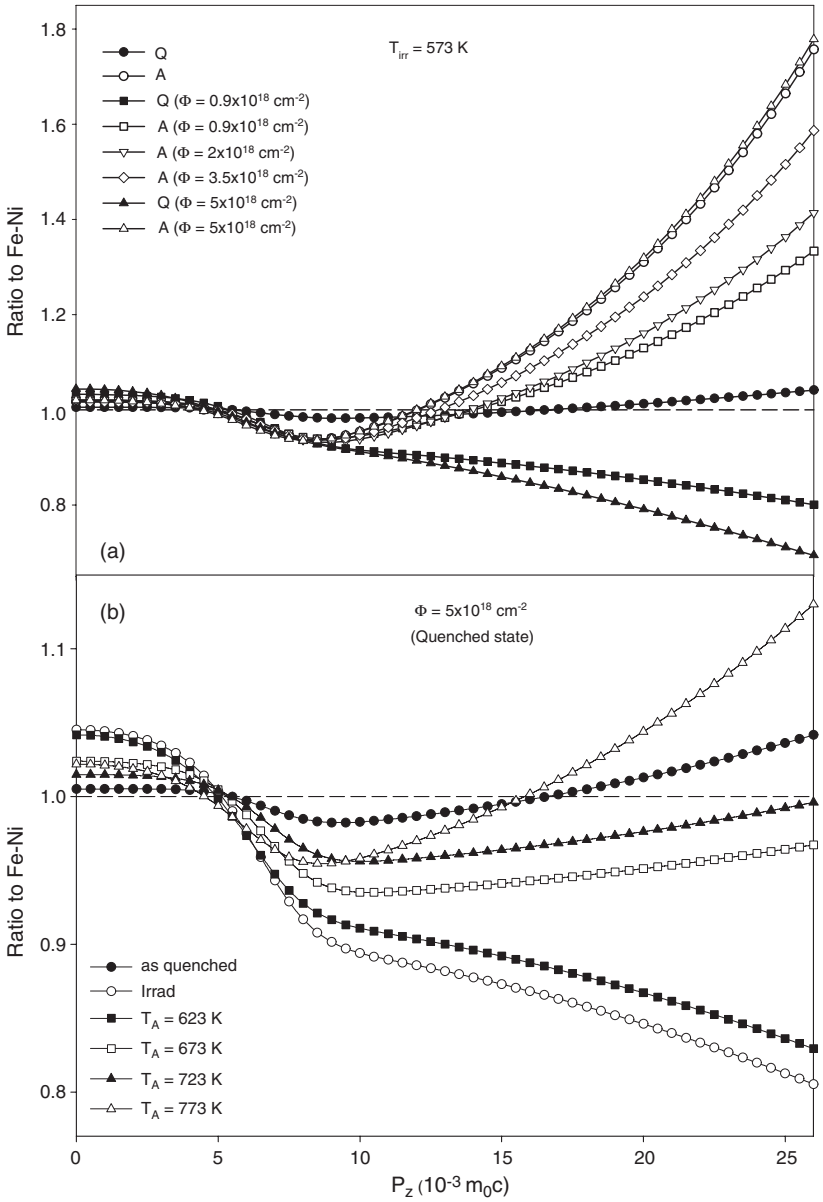

Figure 5. (a) Ratio curves of the ACAR spectra of the Fe–Ni–Al alloys as quenched (Q), after ageing (A), and as irradiated with different electron fluences at 573 K with respect to that of Fe–Ni. (b) Ratio curve variations versus annealing temperature in irradiated Fe–Ni–Al alloy (initial Q-state) at 573 K. For details see the text.

(see figure 5(a)). The situation is quite opposite to the one occurring at lower irradiation temperatures. One may just conjecture that annealing of vacancy defects prevails over their accumulation in the pre-aged alloy exposed to irradiation at 573 K, i.e. defects, which accumulate at small fluences, are annealed during irradiation. Therefore, the fraction of positrons which are trapped at vacancy defects decreases and the curves correspond to states of positrons in nanoparticles.

The decrease in the accumulation of vacancy defects in the pre-aged alloy at this irradiation temperature cannot be estimated quantitatively, because the accumulation is virtually suppressed altogether.

The structure of nanoparticles in the irradiated A-alloy remains unchanged during isochronal annealing at temperatures from 573 to 773 K and the ratio curves fluctuate a little about the initial A-state.

Trapping of positrons in intermetallic nuclei becomes dominant as the annealing temperature of the irradiated alloy in the Q-state increases (see figure 5(b)). After annealing at 773 K the intensity of the curve at $p_z \geqslant 15 \times 10^{-3}\ m_0c$ is higher than the intensity in the initial Q-state. It may be concluded that the size of the nuclei exceeded the critical size for the confinement of positrons [28]. In our opinion, the size of the nuclei increased under irradiation rather than during annealing since similar post-irradiation annealing at lower irradiation temperatures did not lead to the formation of γ'-phase nuclei (see figures 3 and 4). The enhanced growth of γ'-precipitates in Ni-based alloys under irradiation at elevated temperatures is well known [38].

It is probable that the radiation-induced formation of γ'-phase nuclei takes place in the aged alloy too, but this process is disguised by the nanoparticles.

4.2. Possible mechanisms of absorption of point defects by nanoparticles

It was shown in the previous section that nanoparticles like Ni_3Al retard the accumulation of VCs in the Fe–Ni–Al alloy at earlier stages of the radiation damage ($\sim 10^{-4}$ dpa). This effect is enhanced with the irradiation temperature, i.e. when the diffusion path of vacancies is much longer than the distance between nanoparticles ($\sim$20 nm). It should be noted that the influence of nanoparticles is more pronounced during irradiation than annealing (see sections 3.1 and 3.2).

Let us consider probable mechanisms by which intermetallic nanoparticles can influence the evolution of point defects. Unlike incoherent precipitate particles, the perfect coherent γ/γ' interface does not contain defect sites or traps, which serve as sinks for point defects. In this connection, the authors of [3, 39] proposed a qualitative model of a 'forced recombination' of point defects due to their redistribution in fields of elastic stresses arising around coherent precipitates because of the γ/γ' lattice mismatch δ. Ardell *et al* [4] questioned the efficiency of this mechanism on the grounds that in the general case the energy of interaction between point defects and stress fields is low, because the γ/γ' interfacial free energy in Ni-based alloys is small ($<$30 erg cm^{-2}) [40]. However, the effect of γ/γ' interfaces may not be neglected. It is known [16] that the magnitude and the sign of δ correlate with the morphology of particles during coarsening and influence on the creep [41]. Processes of the accumulation of vacancy defects also depend on the magnitude and the sign of δ. Our study [42] demonstrated that Ni_3Ti-type nanoparticles in the fcc Fe–Ni–Ti alloy ($\delta = +0.14\%$ [15]) inhibit the accumulation of vacancy defects during the irradiation at 573 K only. However, the effect of Ni_3Al particles ($\delta = -0.7\%$ [15]) already appears at room temperature. It was also noted [5] that the probability of the recombination of point defects increases at negative δ. Obviously, the interaction between point defects and fields of elastic stresses depends on the interfacial energy. Therefore, more knowledge is needed concerning the dependence of this energy on the temperature, the composition, the size and the shape of the nanoparticles.

Other recombination mechanisms of the loss of point defects to coherent precipitates were discussed too. For example, it was shown [5] that coherent precipitates capture point defects if the formation energy of a Frenkel pair in the matrix is larger than in the precipitates. Unfortunately, it is difficult to estimate the energy ratio of Frenkel pair formation in the matrix and a nanoparticle. The effective vacancy formation enthalpies for Ni_3Al are as high as in

fcc metals, and they increase with increasing Ni content [43]. The theoretical estimates of the interstitial atoms' formation enthalpy is either extremely ambiguous [44] or is lacking altogether.

Unfortunately, our data concerning the decrease in the accumulation of vacancy defects in Fe–Ni–Al alloys which contain nanoparticles do not allow a unique identification of the recombination mechanism of point defects loss. However, if one considers that the influence of nanoparticles on the accumulation of vacancy defects depends on the γ/γ' lattice mismatch δ, one may think that fields of elastic stresses are significant for the enhanced recombination of point defects under irradiation. It is necessary to calculate the energy of interaction between point defects and fields of elastic stresses so as to estimate the efficiency of these fields.

5. Conclusion

The effects of intermetallic particles like Ni_3Al on the evolution of vacancy defects in an fcc Fe–Ni–Al alloy exposed to electron irradiation were studied. It was shown that the presence of homogeneously distributed nanosized (∼4.5 nm) precipitates in the alloy matrix caused a several-fold decrease in the accumulation of vacancies as compared to their accumulation in the quenched alloy. This effect was enhanced with the irradiation temperature. The radiation-induced growth of intermetallic particles was also observed during irradiation at 573 K of a pre-quenched Fe–Ni–Al alloy. Thus, the quantum-dot-like positron state, which we revealed earlier in ultrafine intermetallic particles, provided the control over the evolution of coherent precipitates, along with vacancy defects, during irradiation and annealing. Possible mechanisms of the absorption of point defects by coherent nanoparticles have been discussed.

Acknowledgments

The authors wish to thank Dr N L Pecherkina for her assistance in characterization of the microstructure of the initial solution-annealed and aged samples. This work was supported by the Russian Foundation for Basic Research (project no. 04-02-16053), Federal Agency on Science and Innovation (cipher of work—RI-112/001/298) and the Program of Presidium of RAS 'Basic Problems of Physics and Chemistry Nanosystems'.

References

[1] Williams K R and Fisher S B 1972 *Radiat. Eff.* **15** 243
[2] Johnston W G, Rosolowsky J H, Turkalo A M and Lauritzen T 1974 *J. Nucl. Mater.* **54** 24–40
[3] Parshin A M 1988 *Structure, Strength and Radiation Damage of Corrosion-Resistant Steels Metallurgy* Chelyabinsk (in Russian)
[4] Ardell A J, Mastel B and Laidler J J 1974 *J. Nucl. Mater.* **54** 313–24
[5] Turkin A A and Bakai A S 1999 *J. Nucl. Mater.* **270** 349–56
[6] Eldrup M and Singh B N 1997 *J. Nucl. Mater.* **251** 132–8
[7] Druzhkov A P, Perminov D A, Arbuzov V L, Stepanova N N and Pecherkina N L 2004 *J. Phys.: Condens. Matter* **16** 6395–404
[8] Wendt H and Haasen P 1983 *Acta Metall.* **31** 1649–59
[9] Dupasquier A and Mills A P (ed) 1995 *Positron Spectroscopy of Solids* (Amsterdam: Institute of Physics Publishing)
[10] Berko S 1983 *Positron Solid State Physics* ed W Brandt and A Dupasquier (Amsterdam: North-Holland)
[11] Alatalo M, Kauppinen H, Saarinen K, Puska M J, Makinen J, Hautojarvi P and Nieminen R M 1995 *Phys. Rev.* B **51** 4176–85
[12] Asoka-Kumar P, Alatalo M, Ghosh V J, Kruseman A C, Nielsen B and Lynn K G 1996 *Phys. Rev. Lett.* **77** 2097–100

[13] Druzhkov A P, Gizhevskii B A, Arbuzov V L, Kozlov E A, Shalnov K V, Naumov S V and Perminov D A 2002 *J. Phys.: Condens. Matter* **14** 7981–90
[14] Rempel A A, Sprengel W, Blaurock K, Reichle K J, Major J and Schaefer H-E 2002 *Phys. Rev. Lett.* **89** 185501
[15] Sagaradze V V, Shabashov V A, Lapina T M, Pecherkina N L and Pilyugin V P 1994 *Fiz. Met. Metalloved.* **78** 49–61
Sagaradze V V, Shabashov V A, Lapina T M, Pecherkina N L and Pilyugin V P 1994 *Rus. Phys.—Met. Metallogr.* **78** 619–28 (Engl. Transl.)
[16] Qiu Y Y 1996 *J. Alloys Compounds* **232** 254–63
[17] Morillo J, de Novion C H and Dural J 1981 *Radiat. Eff.* **55** 67
[18] Akshentsev Yu N, Stepenova N N, Sazonova V A and Rodionov D P 1997 *Fiz. Met. Metalloved.* **84** 130–7
Akshentsev Yu N, Stepenova N N, Sazonova V A and Rodionov D P 1997 *Rus. Phys.—Met. Metallogr.* **84** 293–98 (Engl. Transl.)
[19] Arbuzov V L, Danilov S E and Druzhkov A P 1997 *Phys. Status Solidi* a **162** 567–73
[20] Rempel A A, Druzhkov A P and Gusev A I 1989 *Fiz. Met. Metalloved.* **68** 271–9
Rempel A A, Druzhkov A P and Gusev A I 1989 *Sov. Phys.—Met. Metallogr.* **68** 59–68 (Engl. Transl.)
[21] Brandt W 1974 *Appl. Phys.* **5** 1
[22] Nieminen R M and Laakonen J 1979 *Appl. Phys.* **20** 181
[23] Damask A C and Dienes G J 1963 *Point Defects in Metals* (London: Gordon and Breach)
[24] Arbuzov V L, Druzhkov A P and Danilov S E 2001 *J. Nucl. Mater.* **295** 273–80
[25] Puska M J, Lanki P and Nieminen R M 1989 *J. Phys.: Condens. Matter* **1** 6081–93
[26] Puska M J and Nieminen R M 1983 *J. Phys. F: Met. Phys.* **13** 333–46
[27] Nagai Y, Hasegawa M, Tang Z, Hempel A, Yubuta K, Shimamura T, Kawazoe Y, Kawai A and Kano F 2000 *Phys. Rev.* B **61** 6574–8
[28] van Huis M A, van Veen A, Schut H, Falub S V, Eijt S W H, Mijnarends P E and Kuriplach J 2002 *Phys. Rev.* B **65** 085416
[29] Nagai Y, Tang Z, Hassegawa M, Kanai T and Saneyasu M 2001 *Phys. Rev.* B **63** 134110
[30] Siegel R W 1980 *Annu. Rev. Mater. Sci.* **10** 393–425
[31] Wurschum R, Badura-Gergen K, Kummerle E A, Grupp C and Schaefer H-E 1996 *Phys. Rev.* B **54** 849–56
[32] Dlubek G, Brummer O and Hensel E 1976 *Phys. Status Solidi* a **34** 737
[33] Holzwarth U, Barbieri A, Hansen-Ilzhofer S, Schaaff P and Haaks M 2001 *Appl. Phys.* A **73** 467–75
[34] Petegem S V, Zhurkin E E, Mondelaers W, Dauwe C and Segers D 2004 *J. Phys.: Condens. Matter* **16** 591–603
[35] Druzhkov A P, Arbuzov V L and Perminov D A 2002 *Fiz. Met. Metalloved.* **94** 75–9
Druzhkov A P, Arbuzov V L and Perminov D A 2002 *Rus. Phys. —Met. Metallogr.* **94** 68–72 (Engl. Transl.)
[36] Epperson J E, Loomis B A, Faber J Jr, Lin J S and Hendricks R W 1987 *Metall. Trans.* A **18** 2027–35
[37] Epperson J E and Furnrohr P 1983 *Acta Crystallogr.* A **39** 740–6
[38] Ro H and Mitchell T E 1978 *Metall. Trans.* A **9** 1749–60
[39] Nelson R S, Hudson J A, Masey D J, Walters G P and Williams T M 1972 *Radiation-Induced Voids in Metals* (*US AEC Conf. (Albany)*) ed J W Corbett and L C Ianniello p 430
[40] Ardell A J, Nicholson R B and Eshelby J D 1966 *Acta Metall.* **14** 1295–309
[41] MacKay R A, Nathal M V and Pearson D D 1990 *Metall. Trans.* A **21** 381
[42] Druzhkov A P, Arbuzov V L, Perminov D A and Shalnov K V 2003 *Fiz. Met. Metalloved.* **96** 74–8
Druzhkov A P, Arbuzov V L, Perminov D A and Shalnov K V 2003 *Rus. Phys. Met.—Metallogr.* **96** 509–13 (Engl. Transl.)
[43] Badura-Gergen K and Schaefer H-E 1997 *Phys. Rev.* B **56** 3032–7
[44] Wenzl H 1970 Vacancies and interstitials in metals *Proc. Int. Conf. (Julich, Sept. 1968)* Amsterdam, pp 363–423